A New Technique for Enhanced Monochrome Visualization of Non-Visual Data

Andrzej Śluzek[0000−0003−4148−2600]

Warsaw University of Life Sciences, Institute of Information Technology
ul. Nowoursynowska 159 Bld.34, 02-776 Warsaw, Poland
andrzej_sluzek@sggw.edu.pl

Abstract. This paper introduces a novel, unconventional method to enhance the visual clarity of monochrome images derived from non-visual data sources. The approach involves a two-step process: image pseudo-colorization followed by decolorization. Surprisingly, this counterintuitive technique can significantly improve discernibility of image features, irrespective of their size, shape, or original visual prominence. The paper delves into the algorithmic details of this method and presents experimental results on a representative dataset of IR, X-ray, MRI, and ultrasound images. When disregarding factors related to natural image appearance (which are irrelevant in non-visual domains), this method outperforms conventional image enhancement techniques, including sophisticated ones, in terms of standard image quality criteria, i.e., sharpness, contrast, and overall detail perceptibility. This superiority is substantiated by both subjective evaluations and objective metrics. The success of this technique hinges on the careful selection of color maps and the application of a specific, recently proposed decolorization scheme. The technique is well-suited for various visual data analysis tasks in non-visual domains, primarily in AI-based solutions.

Keywords: Non-visual domains · Monochrome images · Image enhancement · Pseudo-coloring · Decolorization.

1 Motivation and Introduction

Grayscale imaging is a widely-used visualization technique for non-visual data that benefits from conversion into 2D images. This method finds application in various domains, mainly in infrared, X-ray (including CT), MRI, and ultrasound imaging. Infrared imaging is particularly valuable in challenging visual conditions, while X-ray, MRI, and ultrasound imaging are essential for non-invasive visualization in fields like biomedical diagnostics and quality control.

In these applications, physical variables such as temperature, reflectivity, radiation absorption or coherent radiation emission are represented by grayscale intensities. This enables the visual detection and classification of scene components based on their grayscale levels. While these visual tasks can be performed

ICCS Camera Ready Version 2025
To cite this paper please use the final published version:
DOI: 10.1007/978-3-031-97564-6_4

by humans (often requiring highly skilled operators), automated systems utilizing advanced identification and classification algorithms, including AI-based approaches, are increasingly taking over.

However, since these images originate from non-visual domains, the grayscale values directly linked to physical variables often hold secondary importance for image content analysis. Prioritizing grayscale values that enhance the perceptibility and prominence of scene components is more crucial, even if those values only indirectly relate to the physical variable of imaging. If needed, the original grayscale values (directly representing temperature, reflectivity, etc.) can be used for further analysis of already identified features or objects. An example in Figures 1(a) and 1(b) shows the original MRI image, and its variant where the grayscale levels are differently assigned but the overall clarity and visual appeal of the image is significantly enhanced.

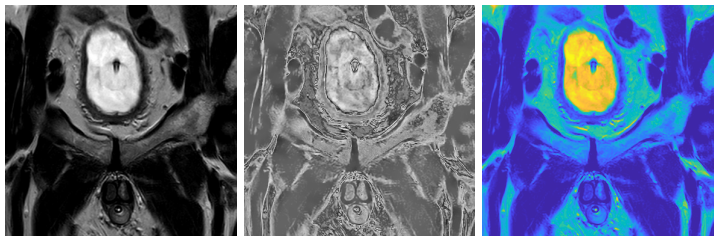

(a) (b) (c)

Fig. 1. Comparison of (a) the original MRI image and (b) the enhanced MRI image obtained using the method proposed in this paper, and (c) the intermediate pseudo-color image (more details to follow) generated during the enhancement process.

In images acquired from natural visual domains, image enhancement employs various processing algorithms (e.g., filters, transform-based approaches, etc.) tailored to specific image categories, often leveraging human visual experiences and expectations. The goal is to improve perceived image quality, which can be defined by multiple factors. Numerous works delve into various aspects of image quality and enhancement, e.g. [3, 5, 13], concluding that overall subjective quality is primarily determined by naturalness, color consistency (inapplicable to monochrome images), sharpness, contrast, and detail perceptibility. Occasionally, certain image characteristics may be undesirable and require correction (e.g., by deblurring, denoising, transfer function compensation, etc.). However, this is usually problem-specific, and the corresponding algorithms are applied selectively.

For monochrome images from non-visual domains, where the concept of naturalness is less applicable, quality enhancement generally follows similar principles, as surveyed in [4, 23]. The objective remains to achieve images that are sharp, well-contrasted, and have clearly discernible details.

ICCS Camera Ready Version 2025
To cite this paper please use the final published version:
DOI: 10.1007/978-3-031-97564-6_4

In this paper, we focus on the challenge of enhancing the discernability of monochrome images acquired from non-visual domains, regardless of their specific physical characteristics or image content. Our approach is novel and, to the best of our knowledge, has not been previously reported in the public domain. Generally, we depart from standard methods such as filtering, transform-based techniques, or contrast enhancement. Instead, we propose a counterintuitive sequence of two operations.

First, the image undergoes pseudo-colorization, a common technique for representing grayscale images from diverse non-visual domains, e.g., [2, 11, 19, 27]. While this technique can enhance the visual appeal of images, it usually fails to significantly improve discernability due to the *one-to-one* mapping between intensities and colors.

In the second step, the pseudo-color image is decolorized into a monochrome image using a recently proposed scheme [22]. This method effectively preserves and enhances fine details from the original color image by incrementally determining pixel intensities based on the colors and intensities of their already processed neighbors. This two-step approach can result in a monochrome image with significantly improved perceptibility compared to both the original grayscale image and the intermediate pseudo-color variant, provided a suitable color map is chosen in the first step.

Figure 1 demonstrates a successful application of this methodology. Conversely, Figure 2 illustrates a case where the final monochrome image shows only minor improvement due to an unsuitable color map choice.

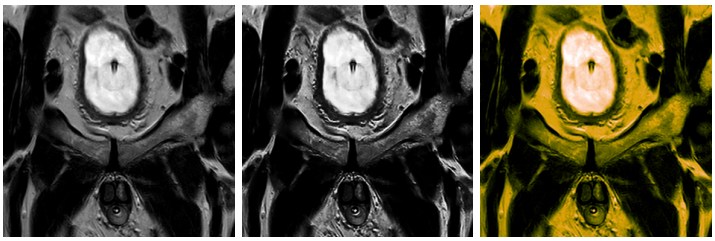

(a) (b) (c)

Fig. 2. Comparison of (a) the original MRI image and (b) the processed MRI image. While the intermediate pseudo-color image (c) is visually appealing, the output monochrome image offers only minor enhancements of discernability. Nevertheless, it does maintain sharper edges than the pseudo-color version.

The remainder of this paper delves into the details of our method for enhancing monochrome images through such an unconventional approach. First, Section 2 presents an overview of the foundational processes, i.e., pseudo-colorization and decolorization. Section 3 describes our methodology in detail, covering the testing procedure, dataset selection, and the subjective and objective quality

ICCS Camera Ready Version 2025
To cite this paper please use the final published version:
DOI: 10.1007/978-3-031-97564-6_4

assessments of the enhanced images. Section 4 summarizes the experimental results, which validate the method. Section 5 discusses its further aspects, and concludes the paper.

2 Foundations

2.1 Image Pseudo-colorization

Pseudo-colorization is a technique that assigns predefined colors to grayscale image intensities. This is achieved through a *color map*, a function that maps intensities to RGB color values. For instance, the *sine* color map employs the following equations:

$$R(I) = -0.5\cos(\pi I) + 0.5,\ G(I) = \sin(\pi I),\ B(I) = 0.5\cos(\pi I) + 0.5. \qquad (1)$$

For standard 8-bit grayscale images, color maps are often implemented as simple lookup tables that map each of the 256 levels to a specific color.

Various color maps are designed to achieve specific visual goals, primarily enhancing aesthetic appeal and content perception in diverse applications [8, 16, 19, 27]. For this study, we selected nine popular color maps with varied characteristics, as depicted in Figure 3. Actually, the *hot* and *jet* maps are included in two slightly different variants, visually indistinguishable but with minor differences in their lookup coefficients. Specifically, Figure 1 employs the *parula* color map, while Figure 2 utilizes the *warm* color map.

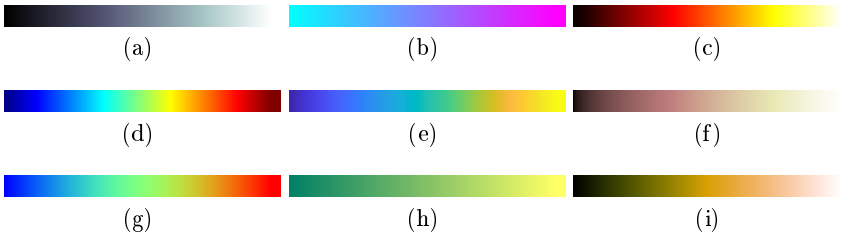

Fig. 3. Popular color maps for pseudo-colorization: (a) *bone*, (b) *cool*, (c) *hot*, (d) *jet*, (e) *parula*, (f) *pink*, (g) *sine*, (h) *summer*, (i) *warm*.

2.2 Decolorization

Decolorization converts color images into grayscale images. Typically, this process involves linear *rgb-to-gray* mappings, represented by the equation

$$I = k_R R + k_G G + k_B B, \qquad (2)$$

where the standard values of $[k_R, k_G, k_B]$ are $[0.299, 0.587, 0.114]$.

ICCS Camera Ready Version 2025
To cite this paper please use the final published version:
DOI: 10.1007/978-3-031-97564-6_4

To address the loss of visual detail that can occur during grayscaling, especially for colors with similar luminance, various methods have been developed over the past two decades. These methods optimize the coefficients in Eq. 2, either globally (e.g., [12, 14, 24, 28]) or locally (e.g., [25, 26]), to enhance the visual expressiveness of the resulting monochrome images.

In [22], a decolorization scheme is proposed that is particularly effective in enhancing contrast in grayscale images compared to their color counterparts, as supported by subjective evaluation and relevant performance metrics. This

.

Fig. 4. Two images from COLOR250 dataset [14] decolorized using the method described in [22].

approach recognizes that a pixel with $[R, G, B]$ color can only be assigned intensities I within the range:

$$min(R, G, B) \leq I \leq max(R, G, B), \tag{3}$$

regardless of the specific values of $[k_R, k_G, k_B]$.

From Eq.3, we identify pixels with the narrowest range of potential intensities. Their grayscale values are randomly chosen from this limited set of options or even assigned deterministically, if $min(R, G, B) = max(R, G, B)$.

These pixels serve as the *initial list* for the decolorization scheme, which is a randomized variant of a popular *flood-fill* algorithm. In this scheme, pixels with decolorized neighbors are assigned grayscale intensities (subject to Eq.3) proportionally to the color differences between themselves and their already decolorized neighbors. This iterative process continues, randomly selecting pixels from the current list and assigning them grayscale values, until the list is emptied, i.e., the entire image is decolorized. For more details, refer to [22].

This scheme produces vivid, high-contrast grayscale images (see examples in Figure 4), outperforming alternative algorithms on benchmark datasets. However, like other local methods, it can introduce spurious artifacts, primarily low-contrast edges, in regions of nearly uniform colors. These artifacts, which tend to appear randomly, can be effectively suppressed by averaging multiple decolorization results. Actual image details remain unaffected by this averaging process.

In the context of the proposed two-step monochrome image enhancement, the advantages of this decolorization method are further discussed in Section 5.2.

ICCS Camera Ready Version 2025
To cite this paper please use the final published version:
DOI: 10.1007/978-3-031-97564-6_4

3 Methodology

3.1 Implementation Framework

To investigate the properties of our method, the following operations are employed:

Initially, each test image is pseudo-colorized using the nine *color maps* detailed in Section 2.1. These intermediate, pseudo-color images are not evaluated or assessed for quality.

.

Fig. 5. Example outdoor IR image (top-left) and its variants processed using 9 color maps (in the order from Fig. 3) and then by 8 standard image processing techniques.

Subsequently, each pseudo-color image is decolorized 15 times using the algorithm outlined in Section 2.2. Averaging multiple decolorizations mitigates potential low-contrast artifacts, as discussed in Section 2.2. The number of iterations is flexible and can be adjusted as needed, as the decolorization algorithm is computationally efficient and has minimal impact on processing time.

Additionally, for reference and comparative purposes, each original monochrome image is processed using eight general-purpose image enhancement methods. We intentionally exclude methods designed for specific tasks, such as noise removal, directional deblurring, or background suppression. Instead, we focus on methods with broad applicability, and varying in complexity, such as:

- histogram equalization;
- Gaussian filtering;
- linear stretching;
- adjustment (i.e., stretching and gamma-correction with extreme intensities clipped);
- contour enhancement (by adding Laplacian edge detector);

ICCS Camera Ready Version 2025
To cite this paper please use the final published version:
DOI: 10.1007/978-3-031-97564-6_4

- LoG filtering;
- sharpening using unsharp masking (e.g., Matlab© `imsharpen` function);
- local Laplacian filtering [18].

Consequently, each test image is represented by 18 variants: the original image, 9 decolorized pseudo-color versions, and 8 standard image processing results. Figure 5 showcases an example of an outdoor IR image and its corresponding 17 processed versions.

3.2 Image Quality Evaluation

The primary objective of this study is to experimentally determine if our proposed method more effectively enhances monochrome images, especially those from non-visual domains, compared to standard image enhancement techniques. To achieve this, we evaluate the quality of the enhanced images using both subjective assessments and metric-based objective analyses. This evaluation is conducted on a dataset of representative images to allow for a statistically significant comparative analysis of various color maps and standard algorithms, as detailed in the subsequent sections.

Subjective Evaluation We first subjectively identify the most perceptually prominent variants for each test image. Three evaluators independently assess the original image and its enhanced variants, selecting the two images with the highest detail discernability. They then collaborate to reach a consensus. Evaluators are instructed to focus solely on the perceivability of image details, regardless of their size, shape, or texture, disregarding any notions of image naturalness.

Figure 6 presents example MRI, X-ray, IR, and ultrasound images, along with their most discernible variants as identified by the evaluators.

Objective Metrics To objectively evaluate image enhancement, we propose three metrics based on well-established image quality assessment concepts. First, we employ the *gradient recall ratio* (GRR, [22, 24]) to estimate the extent to which the overall edge information of the input image I_{in} is preserved ($GRR < 1$) or amplified ($GRR > 1$) in the output image I_{out}.

$$GRR = \frac{\sum_{(x,y)} \sqrt{\partial_x I_{out}(x,y)^2 + \partial_y I_{out}(x,y)^2}}{\sum_{(x,y)} \sqrt{\partial_x I_{in}(x,y)^2 + \partial_y I_{in}(x,y)^2}}. \tag{4}$$

Consistent with previous research (e.g., [9, 10, 17, 21]), we also consider metrics based on image transforms: discrete wavelet transforms (e.g., Haar wavelets) and Fourier (or DCT) transforms. The ratios between the transform coefficients of the output and input images are used as measures of enhancement.

For the Fourier transform, we apply the *FFT recall ratio* (FFTRR):

$$FFTRR = \frac{1}{N} \sum_{(\omega_x,\omega_y)} \frac{|FFT_{out}(\omega_x,\omega_y)|}{|FFT_{in}(\omega_x,\omega_y)|}, \tag{5}$$

ICCS Camera Ready Version 2025
To cite this paper please use the final published version:
DOI: 10.1007/978-3-031-97564-6_4

where coefficients with zero input value ($FFT_{in}(\omega_x, \omega_y) = 0$) are excluded. The DC coefficient $FFT(0,0)$ is also excluded, as it is insignificant for image discernability. N is the number of retained coefficients.

This metric quantifies the amplification of periodic image components, such as textures. It is crucial to recognize that the inherent limited intensity range of monochrome images restricts the excessive amplification of high-magnitude frequencies. Consequently, elevated FFTRR values signify the amplification of lower-amplitude frequencies, thereby increasing their visual prominence.

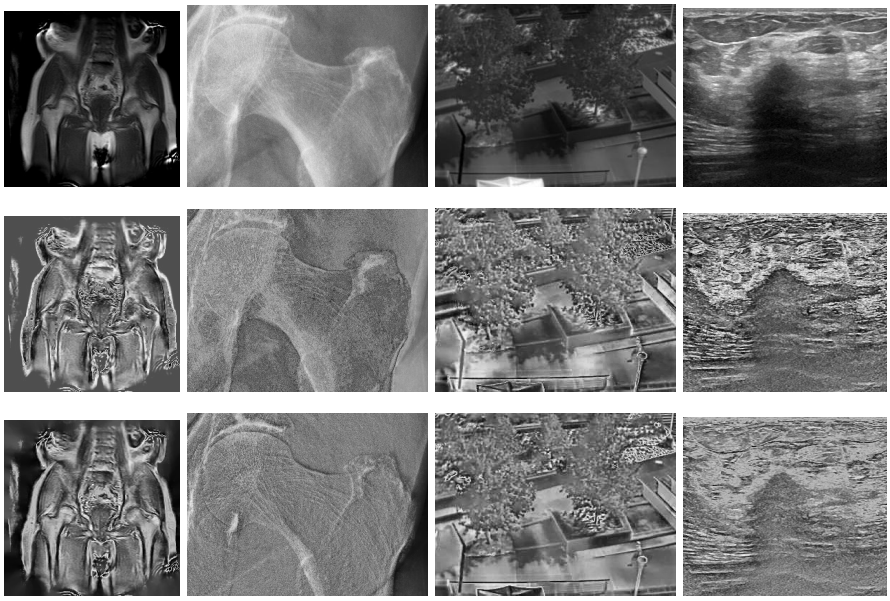

.

Fig. 6. Example MRI, X-ray, IR, and ultrasound images (left to right) and their most discernible variants selected by evaluators.

Finally, two variants of a metric based on the Haar wavelet transform (HWT) are employed to estimate the enhancement in discernability of image fragments across a range of their sizes, shapes and locations.

$$HWTRR1 = \frac{1}{N} \sum_{(j_x, j_y, k_x, k_y)} \frac{|HWT_{out}(j_x, j_y, k_x, k_y)|}{|HWT_{in}(j_x, j_y, k_x, k_y)|}, \tag{6}$$

where coefficients with zero input value, and the DC component of HWT, are excluded. N is again the number of retained coefficients.

As the number of HWT coefficients grows quadratically with the scale number, fine scales, which capture high-frequency details, have a greater impact

ICCS Camera Ready Version 2025
To cite this paper please use the final published version:
DOI: 10.1007/978-3-031-97564-6_4

on the HWTRR1 metric, prioritizing the discernability of small details. Consequently, in the second HWT-based metric, similar results are computed independently for each scale and subsequently averaged across all scales.

$$HWTRR2 = \frac{1}{S}\sum_{s=1}^{S}\left\{\frac{1}{N_s}\sum_{(j_x,j_y,ks_x,ks_y)}\frac{|HWT_{out}(j_x,j_y,ks_x,ks_y)|}{|HWT_{in}(j_x,j_y,ks_x,ks_y)|}\right\}, \quad (7)$$

where S is the number of scales and N_s are numbers of coefficients at each scale.

All metrics utilize the original grayscale image as input, and the output image is generated either by our method or by an alternative image processing algorithm.

3.3 Test Dataset

The performance of our method has been evaluated and compared to general-purpose image enhancement methods on a dataset of IR, X-ray, MRI, and ultrasound images (all figures show images from this dataset).

Given that evaluators had to inspect 18 (or even 27, as explained in Section 5.2) variants of each image, we selected a smaller collection of 132 representative images for subjective quality assessment. Objective metrics were computed for a very large number of images, but all statistics in Section 4 are based on the 132 images to ensure consistency between subjective and objective approaches.

The images were randomly selected from a range of publicly available datasets, including CAMEL [6], FLIR ADAS [1], OTCBVS [7] and KAGGLE [15, 20], as well as from personal collections.

4 Experimental Results

Following the methodology outlined in Section 3, we compare the performances of the image enhancement techniques (i.e., 9 *color maps* and 8 standard image processing algorithms) using both objective and subjective evaluations.

Table 1 presents the mean values of the HWTRR1, HWTRR2, FFTRR, and GRR metrics across the test dataset. The techniques are ranked based on the combined strength (weighted average) of all metrics. The top performers are the *jet*, *sine*, *parula* and *hot* maps, followed by four image enhancement algorithms. The lower part of the table is occupied by less suitable color maps and the remaining algorithms. The last position of the Gaussian filter is unsurprising. As the only (deliberately included) processing algorithm with smoothing characteristics, it cannot enhance the perceivability of fine details and sharp features. This limitation is fully confirmed by its low metric values.

The results of the subjective evaluation align closely with the objective findings. Table 2 shows the overall (i.e., across the entire dataset) contributions of color maps and algorithms to the group of top two images identified by the evaluators.

ICCS Camera Ready Version 2025
To cite this paper please use the final published version:
DOI: 10.1007/978-3-031-97564-6_4

Table 1. Mean values of the metrics across the test dataset.

Rank	Technique	HWTRR1	HWTRR2	FFTRR	GRR
1	*jet* map	5.326	7.263	8.844	2.592
2	*sine* map	3.528	4.948	5.590	2.113
3	*parula* map	3.291	4.035	6.439	1.862
4	*hot* map	2.668	4.148	3.458	2.041
5	local Laplacian	2.893	2.998	3.467	1.766
6	LoG	2.916	3.339	2.190	2.271
7	sharpening	2.917	2.561	3.268	2.252
8	histogram equal.	2.627	3.182	3.036	1.766
9	*warm* map	1.840	2.542	2.520	1.770
10	*cool* map	1.409	3.375	2.464	1.041
11	contour enhancement	2.019	1.840	2.076	1.591
12	adjustment	1.324	1.353	1.403	1.298
13	*pink* map	0.927	1.334	1.298	0.890
14	stretching	1.057	1.057	1.057	1.057
15	*bone* map	0.745	1.188	1.051	0.929
16	*summer* map	0.744	1.192	0.868	0.727
17	Gaussian	0.910	0.973	0.379	0.644

The table is dominated by the same four color maps (*jet*, *sine*, *parula* and *hot*), which collectively contribute 90.32% of the images selected by the evaluators, with only minor or insignificant contributions from other maps or standards algorithms.

Table 2. Images ranked highest in discernibility by evaluators.

Rank	Technique	percentage in top-two images
1	*jet* map	27.58%
2	*sine* map	26.52%
3	*parula* map	18.64%
4	*hot* map	17.58%
5	local Laplacian	4.54%
6	LoG	3.18%
7	*pink* map	0.76%
8	*warm* map	0.61%
9	sharpening	0.30%
10	histogram equal.	0.30%

In summary, we can conclude that the proposed method generally outperforms standard image enhancement methods, provided that color maps are carefully selected in the first step. Incorrectly selected maps offer no improvement.

ICCS Camera Ready Version 2025
To cite this paper please use the final published version:
DOI: 10.1007/978-3-031-97564-6_4

5 Discussion and Conclusions

5.1 Color Maps and Pseudo-color Images

The experimental results in Section 4 clearly demonstrate that the selection of the color map significantly influences the quality of enhanced images. It is crucial to emphasize, however, that the visual characteristics of the pseudo-color images are not directly exploited in our method. The examples in Figures 1, 2 and 7 are provided solely for illustrative purposes. Instead, the color maps serve two critical roles in our method:

(a) For each input intensity, its corresponding pseudo-color determines the range of possible output values (Eq.3).
(b) The distance between intensities is defined as the distance between their respective pseudo-colors, as outlined in Section 2.2 and detailed in [22].

Consequently, in future applications, color maps can be replaced with lookup tables. These tables would directly provide the range of output values for each input intensity (in (a)), and precomputed distances between intensities derived from the color map (in (b)). This substitution would enhance efficiency.

Nonetheless, color maps and pseudo-colored images provide an intuitive approach to explaining the fundamental concepts of the proposed method.

5.2 Significance of Decolorization Algorithm

In another experiment, we investigated the criticality of the decolorization algorithm adapted from [22] in the second step of our method. To this end, we decolorized all pseudo-color images generated in the first step using a standard approach (Eq. 2) with coefficients $[0.299, 0.587, 0.114]$. Analysis revealed that these alternative outputs exhibited a noticeable decline in quality.

Table 3 quantitatively supports this observation, demonstrating a significant deterioration in mean metric values for the top-performing colormaps (*jet*, *sine*, *parula* and *hot*) when the standard decolorization replaced the scheme from [22]. Furthermore, Figure 7 visually illustrates the subjective quality degradation resulting from this substitution. Preliminary experiments with other decolorization models [12, 24] confirmed similar performance declines.

In conclusion, the applied decolorization scheme plays a crucial role in image enhancement, equally important as the selection of the color map.

5.3 Applications in Visual Domains

The proposed method is primarily intended for enhancing monochrome images representing non-visual data. However, it can also be applied to grayscale images of natural scenes. In such cases, image *naturalness* becomes an important factor, and preserving luminance monotonicity is essential. Therefore, for visual domains, we should only consider sequential color maps where the pseudo-colors

ICCS Camera Ready Version 2025
To cite this paper please use the final published version:
DOI: 10.1007/978-3-031-97564-6_4

Table 3. Mean metric values with standard and [22] decolorization.

Color map	HWTRR1 std/ [22]	HWTRR2 std/ [22]	FFTRR std/ [22]	GRR std/ [22]
jet	1.655/5.326	2.250/7.263	2.956/8.844	1.505/2.592
sine	1.158/3.528	1.509/4.948	1.793/5.590	0.989/2.113
parula	0.676/3.291	0.781/4.035	0.897/6.439	0.581/1.862
hot	1.146/2.668	1.307/4.148	1.493/3.458	1.250/2.041

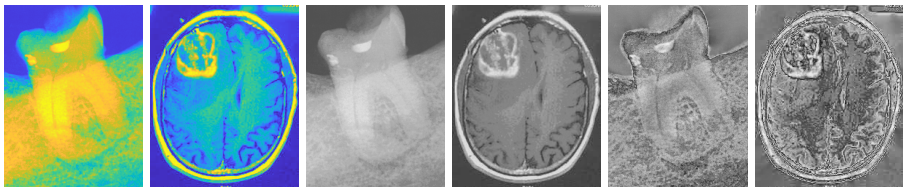

.

Fig. 7. Pseudo-color images and their grayscale counterparts, decolorized using standard (left) and [22] (right) methods.

exhibit monotonic luminance progression (from very dark to very bright). Figure 3 illustrates several such color maps, with the *hot* map being one of the top four identified in Section 4.

Therefore, we applied our method to a selection of natural images employing the *hot* map. The preliminary results, as exemplified in Figure 8, are encouraging.

.

Fig. 8. Example monochrome images of natural scenes enhanced by our method using the *hot* map.

5.4 Summary

The main contribution of this paper is a novel and unconventional method for enhancing the visual clarity of monochrome images derived from non-visual data

ICCS Camera Ready Version 2025
To cite this paper please use the final published version:
DOI: 10.1007/978-3-031-97564-6_4

sources. The approach involves a two-step process: first, pseudo-colorization using carefully selected color maps, followed by decolorization through a specific scheme. Surprisingly, this counterintuitive technique significantly improves the perceptibility of image details, regardless of their size, shape, location, or original visual prominence.

Using a representative dataset of IR, X-ray, MRI, and ultrasound images, we experimentally identified four color maps that consistently outperformed a range of broadly applicable image enhancement algorithms, as demonstrated by both subjective evaluations and objective metrics. However, our study considered only a limited selection of color maps, suggesting that future research could explore additional options with the potential for even greater performance improvements. In fact, approximately 15 other color maps have recently been identified with performances — based on the proposed metrics — comparable to the top four maps identified in this study.

Likewise, we have confirmed that the selection of the decolorization scheme from [22] significantly impacts the method's performance. Determining whether this is the optimal scheme, however, requires further investigation. Toward this end, we might explore developing a mathematical model of the process, though the nonlinearities and random factors in mapping original to output image intensities could present considerable challenges.

Nonetheless, a key avenue for future research is the integration of the proposed method into vision-based diagnostic systems for diverse biomedical applications. We anticipate that improving the discernibility of all image features (regardless of size, shape, location, or initial perceptibility) in monochrome visualizations of ultrasound, X-ray, MRI, and other imaging data can enhance the reliability of decisions made by human diagnosticians and, particularly, by AI-driven systems.

In the illustrative example shown in Figure 9, the outline and structure of a malignant tumor are much clearer in the image enhanced by our method compared to the original USG image.

.

Fig. 9. Outline of a tumor, as identified by a diagnostician, displayed in the original USG image from [20] (left) and in the image enhanced by our method (right).

ICCS Camera Ready Version 2025
To cite this paper please use the final published version:
DOI: 10.1007/978-3-031-97564-6_4

NOTE: All figures are best viewed in high resolution.

Disclosure of Interests. The authors have no competing interests to declare that are relevant to the content of this article.

References

1. FLIR thermal datasets for algorithm training, https://www.flir.com/oem/adas/dataset, accessed on Nov. 12, 2024
2. Aghdam, N.S., Amin, M.M., Tavakol, M.E., Ng, E.: Designing and comparing different color map algorithms for pseudo-coloring breast thermograms. Journal of Medical Imaging and Health Informatics **3**(4), 487–493 (2013). https://doi.org/10.1166/jmihi.2013.1191
3. Beghdadi, A., Larabi, M.C., Bouzerdoum, A., Iftekharuddin, K.: A survey of perceptual image processing methods. Signal Processing: Image Communication **28**(8), 811–831 (2013). https://doi.org/10.1016/j.image.2013.06.003
4. Dabass, J., Vig, R.: Biomedical image enhancement using different techniques - a comparative study. In: Panda, B., Sharma, S., Roy, N.R. (eds.) Data Science and Analytics. pp. 260–286. Springer Singapore, Singapore (2018). https://doi.org/10.1007/978-981-10-8527-7_22
5. Engeldrum, P.G.: A theory of image quality: The image quality circle. Journal of Imaging Science and Technology **48**(6), 447–457 (2004). https://doi.org/10.2352/J.ImagingSci.Technol.2004.48.5.art00012
6. Gebhardt, E., Wolf, M.: CAMEL dataset for visual and thermal infrared multiple object detection and tracking. In: 2018 15th IEEE Int. Conf. AVSS. pp. 1–6 (2018). https://doi.org/10.1109/AVSS.2018.8639094
7. Hammoud, R.I., David, J.W., Fa, G.: OTCBVS benchmark dataset collection (2004-2022), http://vcipl-okstate.org/pbvs/bench, accessed on Oct. 17, 2024
8. Khan, M., Gotoh, Y., Nida, N.: Medical image colorization for better visualization and segmentation. In: Valdés Hernández, M., González-Castro, V. (eds.) Medical Image Understanding and Analysis. pp. 571–580. Springer International Publishing, Cham (2017). https://doi.org/10.1007/978-3-319-60964-5_50
9. Kim, S.E., Jeon, J.J., Eom, I.K.: Image contrast enhancement using entropy scaling in wavelet domain. Signal Processing **127**, 1–11 (2016). https://doi.org/https://doi.org/10.1016/j.sigpro.2016.02.016
10. Krasula, L., Le Callet, P., Fliegel, K., Klíma, M.: Quality assessment of sharpened images: Challenges, methodology, and objective metrics. IEEE Transactions on Image Processing **26**(3), 1496–1508 (2017). https://doi.org/10.1109/TIP.2017.2651374
11. Li, J., Hou, E.S.H.: Pseudocoloring schemes for thermal imaging. In: Grinstein, G.G., Erbacher, R.F. (eds.) Visual Data Exploration and Analysis III. vol. 2656, pp. 77 – 83. SPIE (1996). https://doi.org/10.1117/12.234693
12. Liu, Q., Xiong, J., Zhu, L., Zhang, M., Wang, Y.: Extended RGB2Gray conversion model for efficient contrast preserving decolorization. Multimedia Tools and Applications **76**, 14055–14074 (2017). https://doi.org/10.1007/s11042-016-3748-9
13. Liu, X., Pedersen, M., Wang, R.: Survey of natural image enhancement techniques: Classification, evaluation, challenges, and perspectives. Digital Signal Processing **127**, 103547 (2022). https://doi.org/10.1016/j.dsp.2022.103547

ICCS Camera Ready Version 2025
To cite this paper please use the final published version:
DOI: 10.1007/978-3-031-97564-6_4

14. Lu, C., Xu, L., Jia, J.: Contrast preserving decolorization with perception-based quality metrics. International Journal of Computer Vision **110**, 222–239 (2014). https://doi.org/10.1007/s11263-014-0732-6
15. Mooney, P.: Detecting pneumonia in x-ray images (2017), https://www.kaggle.com/code/paultimothymooney/detecting-pneumonia-in-x-ray-images, accessed on Nov. 12, 2024
16. Moreland, K.: Why we use bad color maps and what you can do about it. In: Proc. IS&T Int'l. Symp. on Electronic Imaging: Human Vision and Electronic Imaging. vol. 28 (2016). https://doi.org/10.2352/ISSN.2470-1173.2016.16.HVEI-133
17. Pappas, T., Safranek, R.: Perceptual criteria for image quality evaluation, pp. 669–684. Academic Press (2000)
18. Paris, S., Hasinoff, S.W., Kautz, J.: Local Laplacian filters: edge-aware image processing with a Laplacian pyramid. Communications of the ACM **58**(3), 81–91 (2015). https://doi.org/10.1145/272369
19. Rahimian, A., Etehadtavakol, M., Moslehi, M., Ng, E.: Comparing different algorithms for the pseudo-coloring of myocardial perfusion single-photon emission computed tomography images. Journal of Imaging **8**(12), 331 (12 2022). https://doi.org/10.3390/jimaging8120331
20. Shah, A.: Breast ultrasound images dataset (2020), https://www.kaggle.com/datasets/aryashah2k/breast-ultrasound-images-dataset, accessed on Nov. 12, 2024
21. Sheikh, H., Bovik, A.: Image information and visual quality. IEEE Transactions on Image Processing **15**(2), 430–444 (2006). https://doi.org/10.1109/TIP.2005.859378
22. Sluzek, A.: Incremental image decolorization with randomizing factors. In: 32nd European Signal Processing Conference (EUSIPCO). pp. 591–595 (2024). https://doi.org/10.23919/EUSIPCO63174.2024.10715444
23. Soundrapandiyan, R., Satapathy, S.C., Chandra Mouli, P.V.S.S.R., Nguyen, G.N.: A comprehensive survey on image enhancement techniques with special emphasis on infrared images. Multimedia Tools and Applications **81**, 9045–9077 (2022). https://doi.org/10.1007/s11042-021-11250-y
24. Wu, T., Eising, C., Glavin, M., Jones, E.: An efficient and effective image decolorization algorithm based on cumulative distribution function. Journal of Imaging **10**(3) (2024). https://doi.org/10.3390/jimaging10030051
25. Wu, T., Toet, A.: Color-to-grayscale conversion through weighted multiresolution channel fusion. Journal of Electronic Imaging **23**(4), 043004 (2014). https://doi.org/10.1117/1.JEI.23.4.043004
26. Yu, J., Li, F., Lv, X.: Contrast preserving decolorization based on the weighted normalized l1 norm. Multimedia Tools and Applications **80**, 31753–31782 (2021). https://doi.org/10.1007/s11042-021-11172-9
27. Zhang, X., Bai, T., Li, H.: Pseudo-color coding method of infrared images based on human vision system. In: Cai, Y., Gong, H., Chatard, J.P. (eds.) Infrared Materials, Devices, and Applications. vol. 6835, p. 68351N. SPIE (2008). https://doi.org/10.1117/12.756471
28. Zhao, R., Liu, T., Xiao, J., Lun, D.P.K., Lam, K.M.: Invertible image decolorization. IEEE Transactions on Image Processing **30**, 6081–6095 (2021). https://doi.org/10.1109/TIP.2021.3091902

ICCS Camera Ready Version 2025
To cite this paper please use the final published version:
DOI: 10.1007/978-3-031-97564-6_4